Hindawi Publishing Corporation
Journal of Chemistry
Volume 2014, Article ID 713573, 7 pages
http://dx.doi.org/10.1155/2014/713573

Research Article

Preparation of Mesoporous SnO_2 by Electrostatic Self-Assembly

Yang Jing, Wang Yan, and Xu Xiaowen

School of Chemistry and Biology Engineering, Jiangsu Key Laboratory for Environment Functional Materials, University of Science and Technology of Suzhou, Suzhou 215009, China

Correspondence should be addressed to Xu Xiaowen; xwxu@mail.usts.edu.cn

Received 12 June 2014; Revised 7 August 2014; Accepted 7 August 2014; Published 21 August 2014

Academic Editor: Fan Dong

We report a simple and scalable strategy to synthesize mesoporous SnO_2 with tin dioxide nanoparticles of 5-6 nm crystalline walls and 3-4 nm pore diameter with the assistance of $Mo_7O_{24}^{6-}$ as templating agent at room temperature. The samples were characterized by XRD, TEM, UV-DRS, XPS, and BET. The product has a moderately high surface area of 132 $m^2\,g^{-1}$ and a narrow mesoporous structure with an average pore diameter of 3.5 nm. The photocatalytic activities of the mesoporous SnO_2 were evaluated by the degradation of methyl orange (MO) in aqueous solution under UV light irradiation.

1. Introduction

Porous SnO_2 has received great attention because of its wide-ranging applications, in areas such as in lithium-ion batteries [1], gas sensors [2], catalysis [3–5], solar cells [6, 7], and supercapacitor electrodes [8] due to its abundance, low cost, and high surface area. Recently, the extensions of soft or/and hard templating procedures to prepare porous SnO_2 with huge specific surface areas have been reported [3]. In order to obtain mesoporous SnO_2, the reported general approach is to use a templating agent, usually a surfactant, which is removed by calcination or chemical extraction after the SnO_2 network is formed. However, the posttreatment, such as high-temperature calcination, may affect the properties of the SnO_2 particles and may reduce the surface areas and pore volume. Therefore, avoiding the use of surfactants is highly desirable and would be beneficial in terms of cost, environmental impact, and scale-up potential. For instance, Mancin and coworkers constructed mesoporous silica through a surfactant-free approach. The templating agent that they used is a hydrolytically unstable inorganic phase and the template could be removed by solvent exchange with water at room temperature [9], but the surface area and pore structure of mesoporous silica had remained unclear.

In this work, we developed a novel, facile, and controllable technique to synthesize mesoporous SnO_2. The technique of electrostatic self-assembly of charged colloidal particles was exploited to prepare mesoporous SnO_2. In our previous works, mesoporous NiO has been fabricated with the assistance of MoO_4^{2-} [10]. Our concept is that two kinds of soluble salt in acidic solution do not hydrolyze. The formation of the homogeneous assemblies is initiated with the generation of a large number of nucleuses after the mixing of the acidic precursor with basic solutions. It is well known that the solubility of $Sn(OH)_4$ in aqueous solution is determined by the pH and the Sn^{4+} concentration. When the pH was adjusted to around 4, the Sn^{4+} ions are almost transformed to colloidal $Sn(OH)_4$

$$Sn^{4+}(aq) + 4OH^{-}(aq) = Sn(OH)_4\,(s) \qquad (1)$$

However, the isoelectric point of colloidal $Sn(OH)_4$ solutions is 4.5 [11]. The pH value that we used (4) was below the isoelectric point of $Sn(OH)_4$; hence the surfaces of $Sn(OH)_4$ colloid are positively charged because of the presence of abundant protonated hydroxyl groups. MoO_4^{2-} ions could be condensed in acid solution, and the extent of condensation depended on the pH level. The dominant species are MoO_4^{2-} ions in pH range of 7–12, and the protonated species were those of $Mo_7O_{24}^{6-}$ ions and of $Mo_8O_{26}^{4-}$ ions in pH ranges 3–5 and at pH below 2, respectively [12]. Therefore, the positively charged $Sn(OH)_4$ and the negatively charged $Mo_7O_{24}^{6-}$

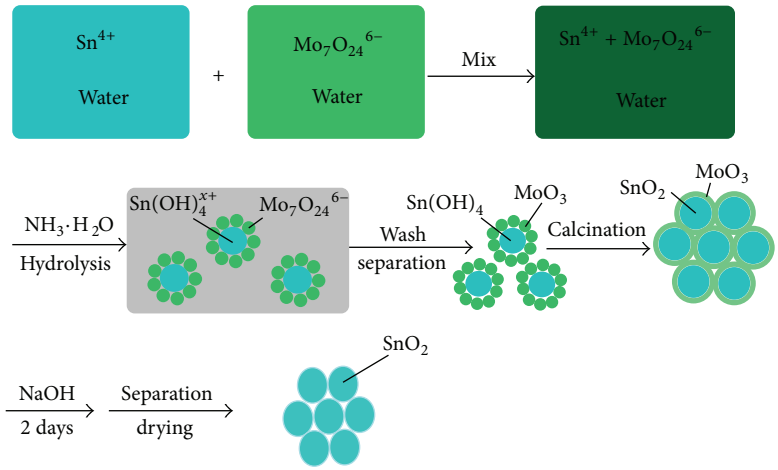

Figure 1: Schematic illustration of the preparation of mesoporous SnO_2.

ions began to coprecipitate (2) when $Mo_7O_{24}^{6-}$ ions were added to colloidal solutions of $Sn(OH)_4$ at a pH value of 4

$$[Sn(OH)_4]^{x+}(s) + \frac{x}{6[Mo_7O_{24}^{6-}]}(aq) = \left[Sn(OH)_4 \cdot \frac{x}{6MoO_4}\right](s)\downarrow \quad (2)$$

Systems of nanoparticles (NPs) interacting through electrostatic forces have been reported. For example, Grzybowski and coworkers reported that large 3D crystals could be prepared by the electrostatic self-assembly of oppositely charged metallic nanoparticles [13]. Crystal growth requires advancing of grain boundaries. Grain boundaries can be "pinned" and hence their motion is restricted by introducing tiny secondary-phase particles along the grain boundaries. The growth of NPs is generally inhibited by surface modification with organic molecules, such as surfactants and ligands [14]. In our system, $Mo_7O_{24}^{6-}$ ions play the role of traditional organic passivating ligands that anchor onto the surface of colloidal $Sn(OH)_4$ particles and form the "pins" at grain boundaries, inhibiting the growth of the particles. Then SnO_2/MoO_3 is formed following the process of separation and calcination. Mesoporous SnO_2 was prepared by dissolving SnO_2/MoO_3 with NaOH solution. Figure 1 illustrates the preparation procedure of mesoporous SnO_2.

2. Experimental Section

2.1. Synthesis. Chemicals: all of the chemicals (analytic reagent, AR) were used as received without further purification.

In a typical experiment, $SnCl_4 \cdot 5H_2O$ (0.02 M) was dissolved in deionized water (50 mL) and produced a clear precursor solution after stirring for 1 h. $(NH_4)_6Mo_7O_{24} \cdot 4H_2O$ (0.0029 M) was dissolved in deionized water (50 mL) to obtain the solution of $(NH_4)_6Mo_7O_{24}$, which was added to the solution of $SnCl_4$ dropwise. After stirring for 30 min, the pH of the solution was adjusted to 4 by dropwise addition of $NH_3 \cdot H_2O$ solution (2 M). The resulting mixture was stirred for an additional 3 h. Then the precipitate was centrifuged and thoroughly washed with deionized water to remove remaining Cl^- and NH_4^+ to obtain the precursor. The precursor was calcined at 400°C in an oven for 3 h with a heating rate of 10°C min^{-1} and then cooled to ambient temperature to obtain $SnO_2@MoO_3$. The SnO_2/MoO_3 was dissolved in NaOH solution (2 M) for 2 days under magnetic stirring, was collected by filtration with a membrane filter, and was dried at 110°C to obtain mesoporous SnO_2.

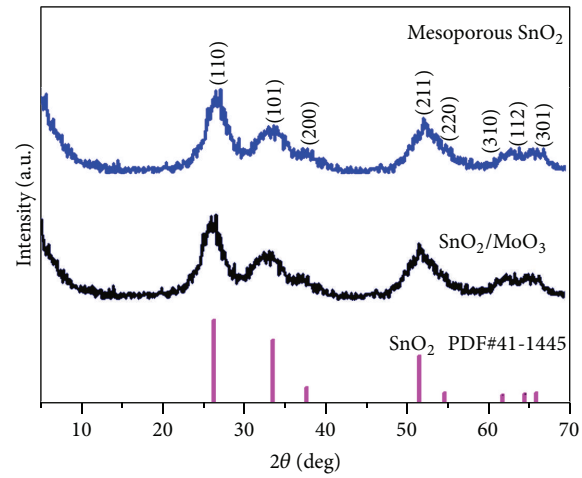

Figure 2: XRD patterns of $SnO_2@MoO_3$ and mesoporous SnO_2.

2.2. Characterizations. The phase structures of as-prepared products were characterized by X-ray diffraction (XRD) (Bruker D8 advance) with Cu-Kα radiation (λ = 1.5418 Å) over a 2θ range between 5° and 70° and the scanning speed of 4° min^{-1} with a step of 0.02°. The sample morphology was examined by transmission electron microscope (TEM) with the accelerating voltage of the electron beam of 200 kV (JEOL JEM-3930EX). Diffuse reflectance spectra (DRS) were obtained for the dry-pressed disk samples using a scan

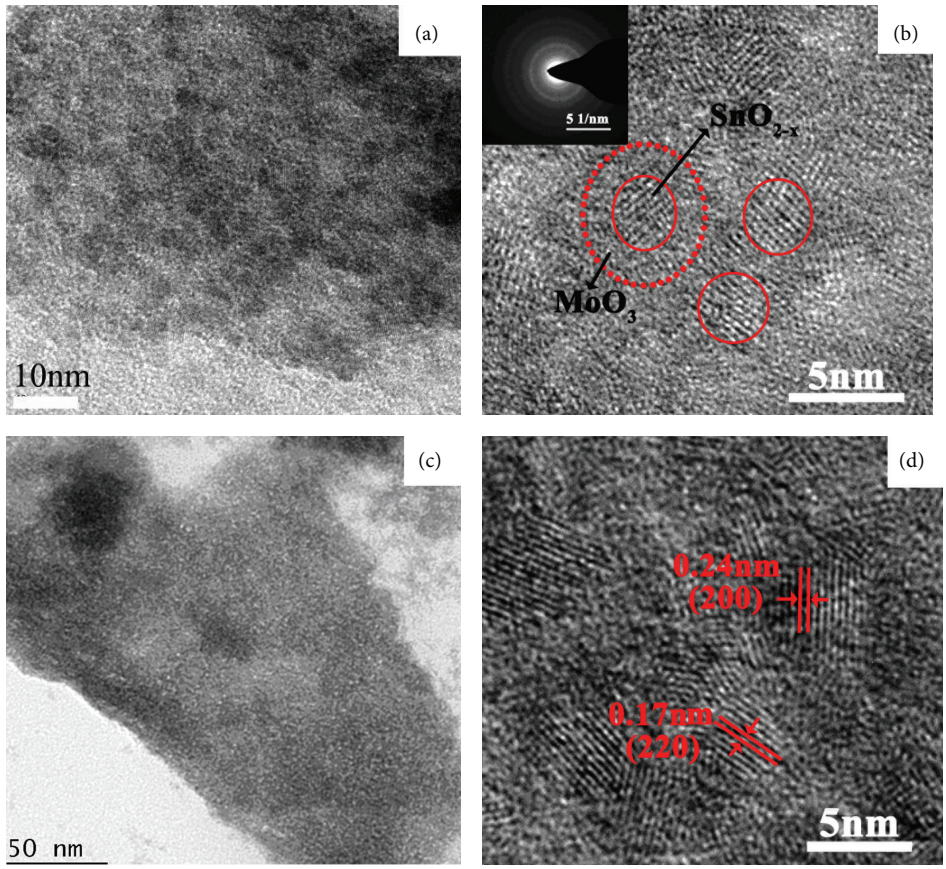

FIGURE 3: (a) TEM image of SnO_2@MoO_3; (b) HRTEM image of SnO_2@MoO_3; (c) TEM image of mesoporous SnO_2; (d) HRTEM images of image of mesoporous SnO_2. Inset shows the corresponding SAED patterns.

UV-vis spectrophotometer (Hitachi U-3010) equipped with an integrating sphere assembly, using $BaSO_4$ as reflectance sample. The spectra were recorded at room temperature in air, in the range of 200–800 nm. Specific surface area and pore diameter of samples were measured by the BET method using N_2 adsorption measurement (ASAP 2020 V3.01H) on nitrogen adsorption at 77 K after the pretreatment at 393 K for 2 h. The specific surface area was calculated by the Brunauer-Emmett-Teller (BET) method, and pore size distribution was obtained from desorption plots by a Barrett-Joyner-Halenda (BJH) analysis. X-ray photoelectron spectroscopy (XPS) spectra were acquired with a Kratos Axis Ultra DLD spectrometer (Kratos Analytical-A Shimadzu group company) using a monochromatic Al Kα source (1486.6 eV). The analyzer uses hybrid magnification mode (both electrostatic and magnetic) and take-off angle is 90°. Under slot mode, the analysis area is 700 × 300 μm. Analysis chamber pressure is less than 5×10^{-9} Torr. Pass energy of 160 eV and 40 eV is normally used for survey spectra and narrow scan spectra, respectively. The BE scale was calibrated according to the C 1s peak (284.8 eV) of adventitious carbon on the analyzed sample surface.

2.3. Measurements of Photocatalytic Activity. The photocatalytic activity of samples was evaluated in terms of the degradation of methyl orange (MO, 10 mg/L). The photocatalyst (0.05 g) was added into a 100 ml quartz photoreactor containing 50 ml of a MO solution. The mixture was stirred for 0.5 h in the dark in order to reach the adsorption-desorption equilibrium. Ultraviolet light was obtained by a 200 W high-pressure mercury lamp with main emission wavelength 313 nm as light source and the distance between the light and the reaction tube is 20 cm. After a given irradiation time, the samples were withdrawn for subsequent analysis with a UV-vis spectrophotometer (Shanghai 760).

3. Results and Discussion

The XRD pattern of the mesoporous SnO_2 is illustrated in Figure 2 to confirm the constitution of the product. It shows eight characteristic diffraction peaks at 26.6°, 33.9°, 37.9°, 51.8°, 54.8°, 61.9°, 64.7°, and 65.9°, corresponding to the (110), (101), (200), (211), (220), (310), (112), and (301) crystalline planes of SnO_2 (JCPDS card number 41-1445). No diffraction peaks of other impurities were detected, indicating that MoO_3 exists in the product in amorphous form. The crystallite size calculated from the widened (110) diffraction peak at $2\theta = 26.6°$ according to the Scherrer equation is 5.1 nm, which is in good accord with the thickness observed on HRTEM (Figure 3).

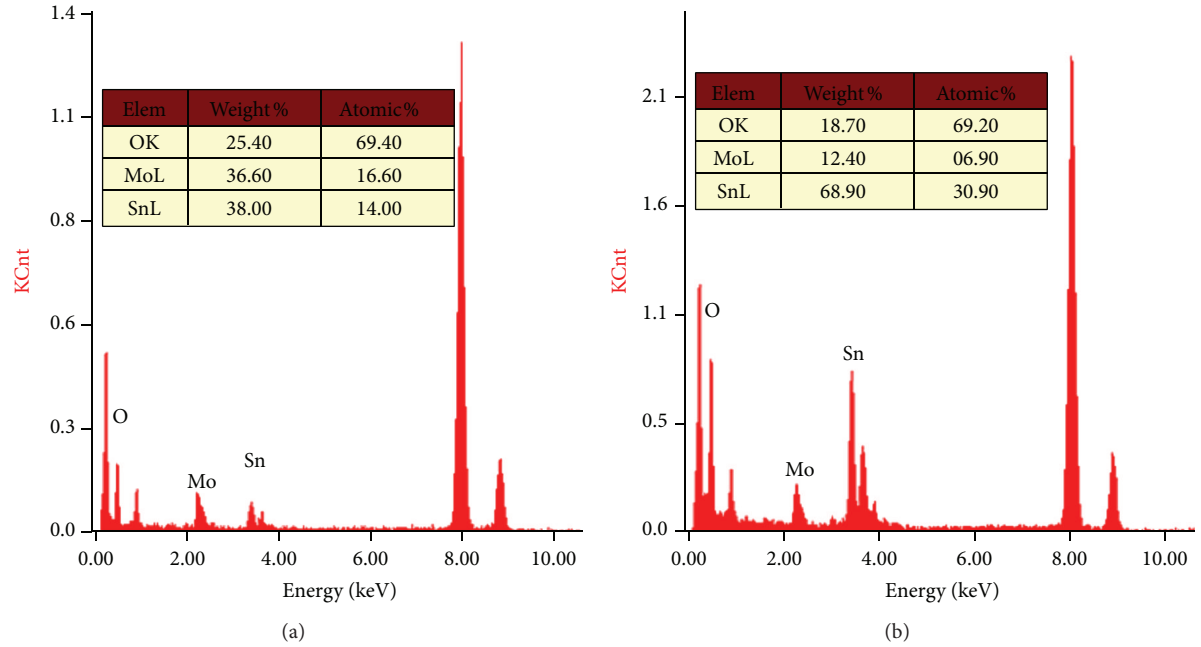

Figure 4: The EDX patterns of the content of Mo atoms in SnO_2@MoO_3 (a) and mesoporous SnO_2 (b).

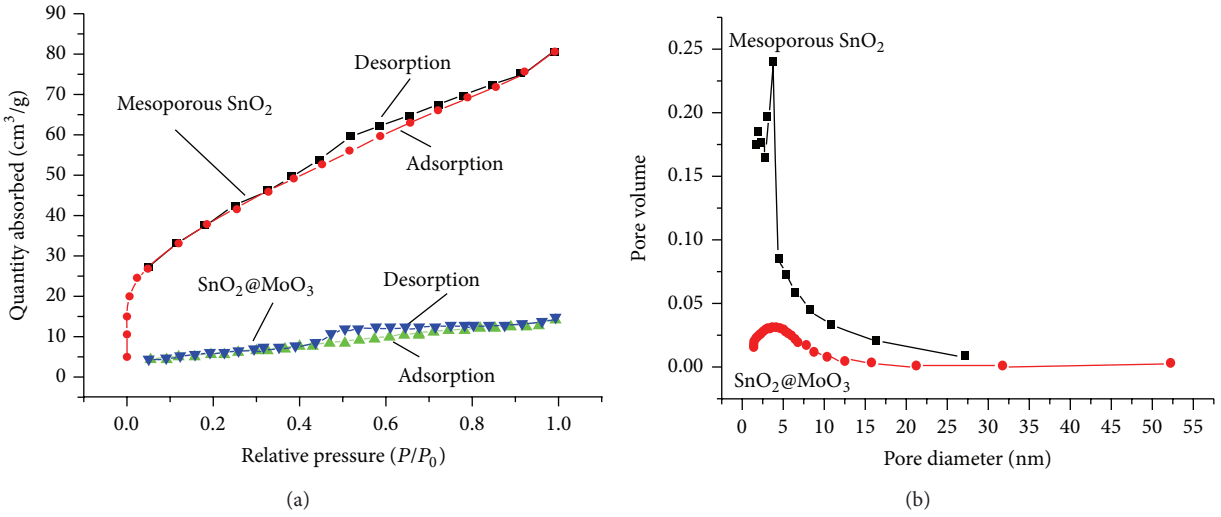

Figure 5: Nitrogen adsorption-desorption isotherm (a) and pore size distribution (b).

The morphology and microstructure of the prepared SnO_2@MoO_3 and mesoporous SnO_2 were examined by TEM measurements. Figures 3(a) and 3(b) show representative SnO_2@MoO_3 samples and Figures 3(c) and 3(d) show representative mesoporous SnO_2, which aggregated from ultrafine nanoparticles with a typical diameter of 6 nm. It can be clearly seen that amorphous MoO_3 layer was coated onto SnO_2 nanoparticles in SnO_2@MoO_3 in Figure 3(b), confirming that the formation mechanism of SnO_2/MoO_3 is exactly as described in Figure 1. The SnO_2 nanoparticles with a size of about 5-6 nm can be identified. The SAED (inset of Figure 3(b)) image presents the polycrystalline behavior of the materials due to the spot and ring patterns. The spacing between two adjacent lattice fringes are 0.24 nm and 0.17 nm, corresponding well to the spacing of the (200) and (220) plane of SnO_2 (Figure 3(d)), respectively. This is perfectly in agreement with the XRD analytical results. Since SnO_2 is insoluble and MoO_3 is highly soluble in NaOH solution, the content of Mo atoms in SnO_2@MoO_3 is reduced from 16.6% before dissolution to 6.9% after dissolution in NaOH solution (Figure 4), which suggests that $Mo_7O_{24}^{6-}$ plays the role of the protective and stabilizing agent coated onto SnO_2 to inhibit the growth of the particles during calcination.

The nitrogen adsorption-desorption isotherm (a) and BJH-derived pore size distributions (b) of the sample are shown in Figure 5. Its micro/mesoporous properties are

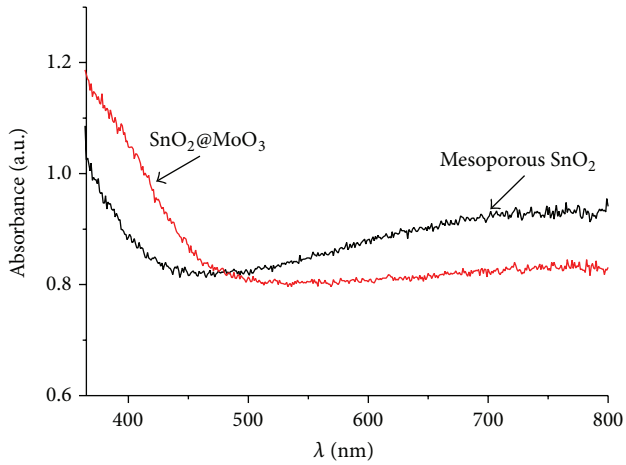

Figure 6: Diffuse reflectance spectra of SnO_2/MoO_3 and mesoporous SnO_2.

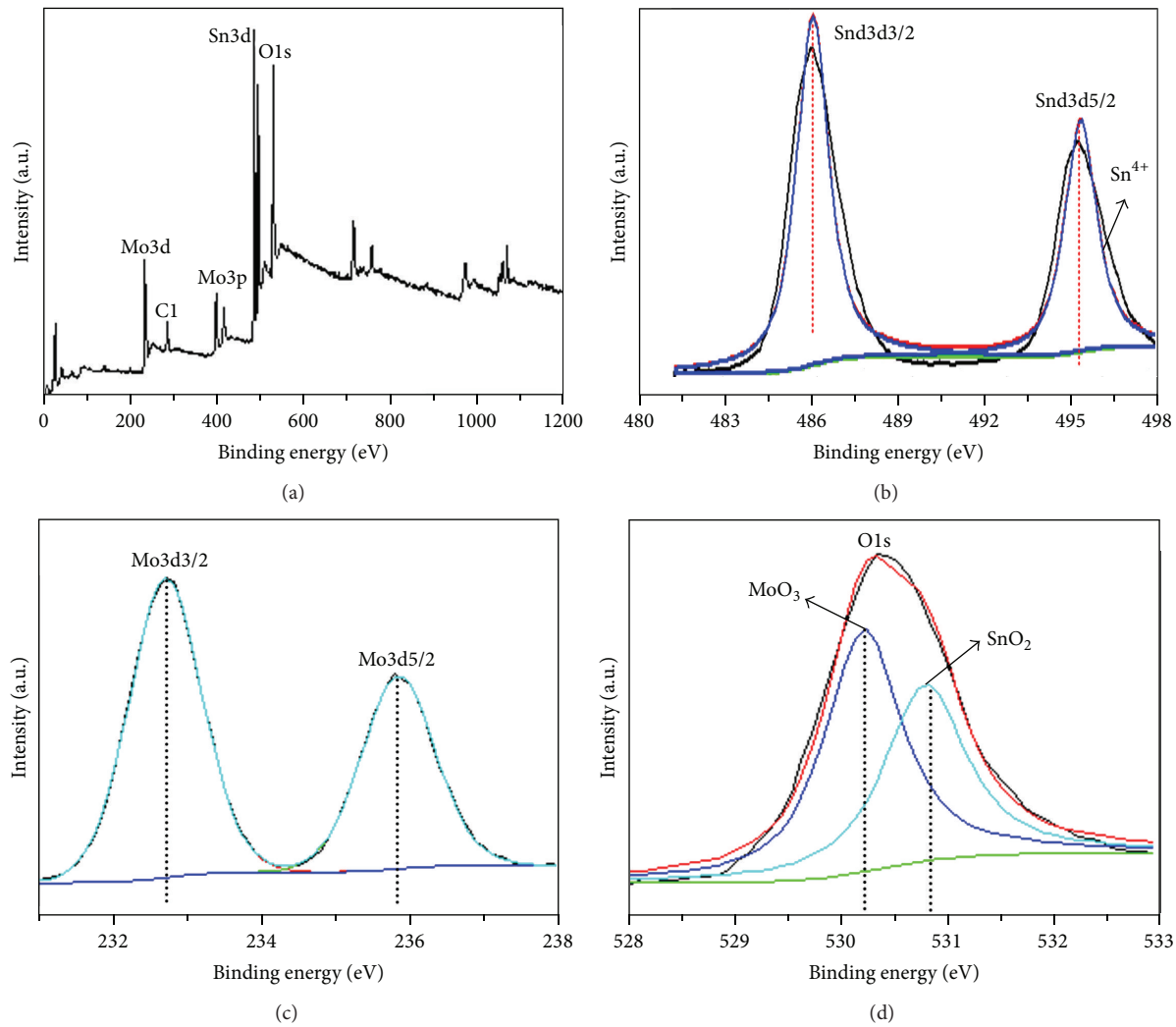

Figure 7: (a) XPS survey spectra of mesoporous SnO_2. High-resolution XPS of (b) Sn3d, (c) Mo3d, and (d) O1s spectra.

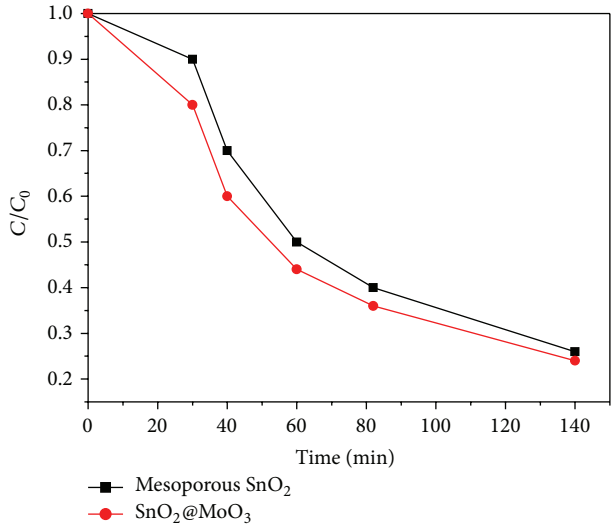

FIGURE 8: Photodegradation of MO under ultraviolet light irradiation by SnO_2@MoO_3 and mesoporous SnO_2.

indicated by the hybrid isotherm (I + IV) type in Figure 5(a). The sample has a BET surface area of 132 $m^2 g^{-1}$, a narrow mesoporous structure with an average pore diameter (Figure 3(b)) of 3.5 nm, and a pore volume of 0.12 $cm^3 g^{-1}$. The BET surface area of samples increased to 132 $m^2 g^{-1}$ from 21 $m^2 g^{-1}$, and the average pore diameter reduced from 4.2 nm to 3.5 nm after dissolution with NaOH, which suggests that MoO_3 plays the role of the protective and stabilizing agent coated onto SnO_2 to inhibit the growth of the particles during calcinations.

The diffuse reflectance spectra of the samples show photoresponse in visible light region (Figure 6). The absorption edge of mesoporous SnO_2 is estimated to be 420 nm with a band gap of 3.0 eV, which is less than the bulk band gap (3.6 eV). Meanwhile, it can be clearly observed that SnO_2@MoO_3 exhibits a higher absorbance in the visible light range than mesoporous SnO_2. This may be caused by the fact that MoO_3 shell can serve as a component in the composites and the interfacial coupling effect between MoO_3 and SnO_2 particles is possibly for the red-shift of the band gap. Such an enhancement in the visible light harvesting, including absorbance and scattering, can increase the number of photogenerated electrons and holes to participate in the photocatalytic reaction and enhance the photocatalytic performance [15].

The surface chemical composition and chemical states of mesoporous SnO_2 were further confirmed by X-ray photoelectron spectroscopy (XPS). Only Sn, Mo, C, and O species were detected (Figure 7(a)). In Figure 7(b), the Sn3d5 binding energy peaks are observed at ~486.7 and ~495.1 eV, corresponding to the spin orbit of Sn3d5/2 and Sn3d3/2, which suggests that Sn in the samples exists in a tetravalent-oxidation state [16]. The Mo 3d core level spectrum of the MoO_3 consists of a spin orbit doublet with peaks at 232.6 and 235.8 eV, associated with Mo cations in the higher oxidation state (Mo^{6+}) (Figure 7(c)) [17]. Additionally, the peak with an O1s binding energy around 530.8 eV is attributed to oxygen in the SnO_2 crystal lattice, which corresponds to the Sn–O–Sn bonds [18], while the other peak positioned at 530.4 eV should be ascribed to the typical Mo–O bond [19].

The photocatalytic activities of the investigated samples were evaluated by measuring the time-dependent degradation of MO in an aqueous catalyst suspension. Figure 8 illustrates the relative concentration C/C_0 of MO as a function of time under ultraviolet light irradiation in the presence of the catalysts. Prior to irradiation, the suspension of the catalyst and dye solution was stirred in the dark for 0.5 hours to reach the equilibrium adsorption. It was noteworthy that the adsorption of MO was found to gradually increase with the increase of Mo content and MO could be completely decolorized after 2.5 hours.

In order to evaluate the photocatalytic activity of the synthesized mesoporous SnO_2, photocatalytic degradation of methylene blue (MB) was also studied under ultraviolet light irradiation. Mesoporous SnO_2 also performed on photocatalytic activity of degradation of MO. The effect of the pH value of the MO solution on the photocatalytic activity of mesoporous SnO_2 was tested. It can be observed that the pH value can significantly affect the photocatalytic activity. The degradation rates are 60% and 100% under the conditions of pH = 4 and pH = 7, respectively, while it is only 10% when the pH value is further increased to 9.

4. Conclusion

In summary, we have synthesized SnO_2 nanoparticles 5-6 nm in size with the assistance of $Mo_7O_{24}^{6-}$ in aqueous solution at room temperature and assembled them into mesoporous materials. Mesoporous SnO_2 shows photocatalytic activities by the degradation of MO in aqueous solution under UV light irradiation.

Conflict of Interests

The authors declare that there is no conflict of interests regarding the publication of this paper.

References

[1] L. Y. Jiang, X. L. Wu, Y. G. Guo, and L. J. Wan, "SnO_2-based hierarchical nanomicrostructures: facile synthesis and their applications in gas sensors and lithium-ion batteries," *The Journal of Physical Chemistry C*, vol. 113, no. 2, pp. 14213–14219, 2009.

[2] P. Manjula, R. Boppella, and S. V. Manorama, "A facile and green approach for the controlled synthesis of porous SnO_2 nanospheres: application as an efficient photocatalyst and an excellent gas sensing material," *ACS Applied Materials & Interfaces*, vol. 4, no. 11, pp. 6252–6260, 2012.

[3] Q. Q. Wang, B. Z. Lin, B. H. Xu, X. L. Li, Z. J. Chen, and X. T. Pian, "Preparation and photocatalytic properties of mesoporous SnO_2-hexaniobate layered nanocomposite," *Microporous and Mesoporous Materials*, vol. 130, no. 1–3, pp. 344–351, 2010.

[4] X. Wang, H. Q. Fan, and P. R. Ren, "Electrospinning derived hollow SnO_2 microtubes with highly photocatalytic property," *Catalysis Communications*, vol. 31, pp. 37–41, 2013.

[5] X. J. Liu, L. K. Pan, T. Q. Chen et al., "Visible light photocatalytic degradation of methylene blue by SnO_2 quantum dots prepared via microwave-assisted method," *Catalysis Science & Technology*, vol. 3, no. 7, pp. 1805–1809, 2013.

[6] M. A. Hossain, G. Yang, M. Parameswaran, J. R. Jennings, and Q. Wang, "Mesoporous SnO_2 spheres synthesized by electrochemical anodization and their application in CdSe-sensitized solar cells," *Journal of Physical Chemistry C*, vol. 114, no. 49, pp. 21878–21884, 2010.

[7] G. L. Shang, J. H. Wu, M. L. Huang et al., "Facile synthesis of mesoporous tin oxide spheres and their applications in dye-sensitized solar cells," *Journal of Physical Chemistry C*, vol. 116, no. 38, pp. 20140–20145, 2012.

[8] J. Yan, E. Khoo, A. Sumboja, and P. S. Lee, "Facile coating of manganese oxide on tin oxide nanowires with high-performance capacitive behavior," *ACS Nano*, vol. 4, no. 7, pp. 4247–4255, 2010.

[9] L. Bau, B. Bartova, M. Arduini, and F. Mancin, "Surfactant-free synthesis of mesoporous and hollow silica nanoparticles with an inorganic template," *Chemical Communications*, no. 48, pp. 7584–7586, 2009.

[10] H. Chen, J. L. Xu, X. W. Xu, and Q. L. Zhang, "Preparation of mesoporous NiO with excellent pseudocapacitive behavior," *European Journal of Inorganic Chemistry*, vol. 2013, no. 7, pp. 1105–1108, 2013.

[11] G. A. Parks, "The isoelectric points of solid oxides, solid hydroxides, and aqueous hydroxo complex systems," *Chemical Reviews*, vol. 65, pp. 177–198, 1965.

[12] C. V. Krishnan, M. Garnett, B. Hsiao, and B. Chu, "Electrochemical measurements of isopolyoxomolybdates: 1. pH dependent behavior of sodium molybdate," *International Journal of Electrochemical Science*, vol. 2, pp. 29–51, 2007.

[13] A. M. Kalsin, M. Fialkowski, M. Paszewski, S. K. Smoukov, K. J. M. Bishop, and B. A. Grzybowski, "Electrostatic self-assembly of binary nanoparticle crystals with a diamond-like lattice," *Science*, vol. 312, no. 5772, pp. 420–424, 2006.

[14] Y. Oaki, K. Nakamura, and H. Imai, "Homogeneous and disordered assembly of densely packed titanium oxide nanocrystals: an approach to coupled synthesis and assembly in aqueous solution," *Chemistry—A European Journal*, vol. 18, no. 10, pp. 2825–2831, 2012.

[15] T. G. Xu, L. W. Zhang, H. Y. Cheng, and Y. F. Zhu, "Significantly enhanced photocatalytic performance of ZnO via graphene hybridization and the mechanism study," *Applied Catalysis B: Environmental*, vol. 101, pp. 382–387, 2011.

[16] H. J. Ahn, H. C. Choi, K. W. Park, S. B. Kim, and Y. E. Sung, "Investigation of the structural and electrochemical properties of size-controlled SnO_2 nanoparticles," *The Journal of Physical Chemistry B*, vol. 108, no. 28, pp. 9815–9820, 2004.

[17] W. Grünert, A. Y. Stakheev, R. Feldhaus, K. Anders, E. S. Shpiro, and K. M. Minachev, "Analysis of Mo(3d) XPS spectra of supported Mo catalysts: an alternative approach," *Journal of Physical Chemistry*, vol. 95, no. 3, pp. 1323–1328, 1991.

[18] S. Wu, S. Yuan, L. Y. Shi, Y. Zhao, and J. H. Fang, "Preparation, characterization and electrical properties of fluorine-doped tin dioxide nanocrystals," *Journal of Colloid and Interface Science*, vol. 346, no. 1, pp. 12–16, 2010.

[19] M. Vasilopoulou, A. M. Douvas, D. G. Georgiadou et al., "The influence of hydrogenation and oxygen vacancies on molybdenum oxides work function and gap states for application in organic optoelectronics," *Journal of the American Chemical Society*, vol. 134, no. 39, pp. 16178–16187, 2012.